© 2014. Published by The Company of Biologists Ltd | Development (2014) 141, 1095-1103 doi:10.1242/dev.098855

RESEARCH ARTICLE

The neural crest cell cycle is related to phases of migration in the head

Dennis A. Ridenour[1], Rebecca McLennan[1], Jessica M. Teddy[1], Craig L. Semerad[1], Jeffrey S. Haug[1] and Paul M. Kulesa[1,2,*]

ABSTRACT

Embryonic cells that migrate long distances must critically balance cell division in order to maintain stream dynamics and population of peripheral targets. Yet details of individual cell division events and how cell cycle is related to phases of migration remain unclear. Here, we examined these questions using the chick cranial neural crest (NC). *In vivo* time-lapse imaging revealed that a typical migrating NC cell division event lasted ~1 hour and included four stereotypical steps. Cell tracking showed that dividing NC cells maintained position relative to non-dividing neighbors. NC cell division orientation and the time and distance to first division after neural tube exit were stochastic. To address how cell cycle is related to phases of migration, we used FACs analysis to identify significant spatiotemporal differences in NC cell cycle profiles. Two-photon photoconversion of single and small numbers of mKikGR-labeled NC cells confirmed that lead NC cells exhibited a nearly fourfold faster doubling time after populating the branchial arches. By contrast, Ki-67 staining showed that one out of every five later emerging NC cells exited the cell cycle after reaching proximal head targets. The relatively quiescent mitotic activity during NC cell migration to the branchial arches was altered when premigratory cells were reduced in number by tissue ablation. Together, our results provide the first comprehensive details of the pattern and dynamics of cell division events during cranial NC cell migration.

KEY WORDS: Neural crest, Chick, Cell division, Cell cycle, Migration, Time lapse

INTRODUCTION

Cell proliferation plays a significant role during embryonic development. When subpopulations of cells are required to travel long distances in the embryo to pattern peripheral tissues, cell division and migration events must be tightly integrated (Aman and Piotrowski, 2011; Kulesa and Gammill, 2010; Solnica-Krezel and Sepich, 2012; Tarbashevich and Raz, 2010). The disruption of either process may lead to developmental malformations and tumor growth (Cordero et al., 2011; Trainor, 2010; Wu et al., 2010). Typical techniques to analyze cell division events and cell cycle during embryonic development have been limited to studying snapshots of cells in fixed tissue. For example, cells may be fluorescently marked to distinguish the G1, G2/S or M phases of the cell cycle, but mitotic patterns are extrapolated from static images. Thus, static techniques severely limit our ability to understand the dynamic nature of an individual cell division event and cell cycle patterns during embryogenesis.

Novel reporters now permit a dynamic readout of cell cycle phase by linking cell cycle proteins active in G1 or G2/S with distinct fluorescence signals visualized using 3D live cell time-lapse imaging (Ridenour et al., 2012; Sakaue-Sawano et al., 2008). However, these reporters have their own limitations, including the challenge of accurately identifying the cytoplasmic-to-nuclear transition of fluorescence during cell cycle changes (Hahn et al., 2009) or functionality in only a limited number of model systems (Abe et al., 2013; Sugiyama et al., 2009). Alternatively, refinements in time-lapse imaging, either with multi-position epifluorescence microscopy or multicolor cell labeling, highlight the strengths of dynamic *in vivo* imaging to better characterize cell division events (Kulesa et al., 2010). For example, during embryonic development, this may include gastrulation (Gong et al., 2004; Quesada-Hernández et al., 2010) and cardiovascular development (Sato et al., 2010). Thus, *in vivo* dynamic imaging provides an important tool to visualize cell division and migration.

The highly migratory neural crest (NC) is an excellent model with which to study the relationship between cell cycle and phases of migration during vertebrate development. In the head, NC cells exit the dorsal neural tube, undergo directed migration along stereotypical pathways, and populate the face and branchial arches (Kulesa and Gammill, 2010). Cranial NC cells contribute to multiple head structures, including bone and cartilage, cranial ganglia and the eye (Creuzet et al., 2005; d'Amico-Martel and Noden, 1980; Gage et al., 2005; Hamburger, 1961; Le Douarin and Kalcheim, 1999; Schlosser, 2006). Failure of NC cells to balance cell division and migration events properly may result in a number of birth defects, termed neurocristopathies (Carstens, 2004; Kouskoura et al., 2011). Thus, studies of the NC may lead to important insights about the cellular and molecular mechanisms that underlie complex patterning events in the vertebrate embryo.

One of the major questions in NC cell biology is how is the cell cycle related to the three distinct phases of NC cell migration. This includes acquisition of direction, homing to and invasion of peripheral targets (Kulesa et al., 2010). A previous static study (using BrdU labeling) of cranial NC cell delamination showed that chick cranial NC cells exit the neural tube in random phases of the cell cycle (Théveneau et al., 2007). However, subsequent details of the dynamics of individual NC cell division events during migration and population of head targets were not examined. Some insights into NC cell division events during migration have come from studies of enteric nervous system development. During chick enteric NC cell migration, cells preferentially divide within the migratory front to drive a tissue-scale invasion (Landman et al., 2011; Simpson et al., 2007). Whether frontal expansion is a general characteristic within other NC cell migratory streams is unknown.

[1]Stowers Institute for Medical Research, 1000 East 50th Street, Kansas City, MO 64110, USA. [2]Department of Anatomy and Cell Biology, University of Kansas School of Medicine, 3901 Rainbow Boulevard, Kansas City, KS 66160, USA.

*Author for correspondence (pmk@stowers.org)

Received 9 May 2013; Accepted 15 December 2013

Development (2014) doi:10.1242/dev.098855

In a previous study, we used *in ovo* photoactivation to mark subregions of the chick cranial NC cell migratory streams and found that lead NC cells increased in number by eightfold (and threefold higher, relative to trailing NC cells) between the time of neural tube exit and population of the branchial arches (Kulesa et al., 2008). These static experiments suggested that frontal expansion may drive cranial NC cell invasion. However, details of individual cranial NC cell division dynamics and cell cycle progression during migration remained unclear.

In this study, we examine the complex cell dynamics and pattern of cranial NC cell division events using *in vivo* dynamic imaging. We address whether NC cell proliferation and cell cycle progression are related to phases of migration in the head. Using time-lapse confocal microscopy, we measure cell velocity profiles during cell division events, time and position to first division, and cell division orientation after cranial NC cells exit the neural tube. We calculate the number of progeny derived from single and small numbers of cranial NC cells using two-photon photoconversion. To determine cell cycle profiles during distinct phases of cranial NC cell migration, we use FACS analysis and Ki-67 staining. We also ask whether stream density affects NC cell proliferation using tissue ablation to decrease the number of migrating cells. Our results represent the first comprehensive *in vivo* details of cranial NC cell proliferation dynamics and the relationship between the NC cell cycle and phases of migration.

RESULTS

Time-lapse analysis revealed a four-step sequence to a neural crest cell division event during migration

To determine the dynamics of an individual NC cell division event during migration, we examined cell behaviors after neural tube exit through invasion of peripheral head targets (Fig. 1; supplementary material Movie 1). *In vivo* confocal time-lapse imaging (n=14 time-lapse imaging sessions) revealed a four-step sequence to a stereotypical NC cell division event, lasting ~1 hour (Table 1, total length of mitosis=59.2±6.0 minutes, n=19 divisions). First, each dividing NC cell retracted its cell protrusions (Fig. 1A, yellow, 17.2±2.2 minutes). Second, dividing NC cells rounded-up and underwent cytokinesis (Fig. 1A, red, 19.0±1.8 minutes). Third, daughter NC cells re-extended protrusions (Fig. 1A, green, 23.0±3.7 minutes) and finally, resumed directed migration (Fig. 1A, orange). These four distinct NC cell division steps were consistent in both *in vivo* (Fig. 1A; Table 1) and *in vitro* migrating cranial NC cells.

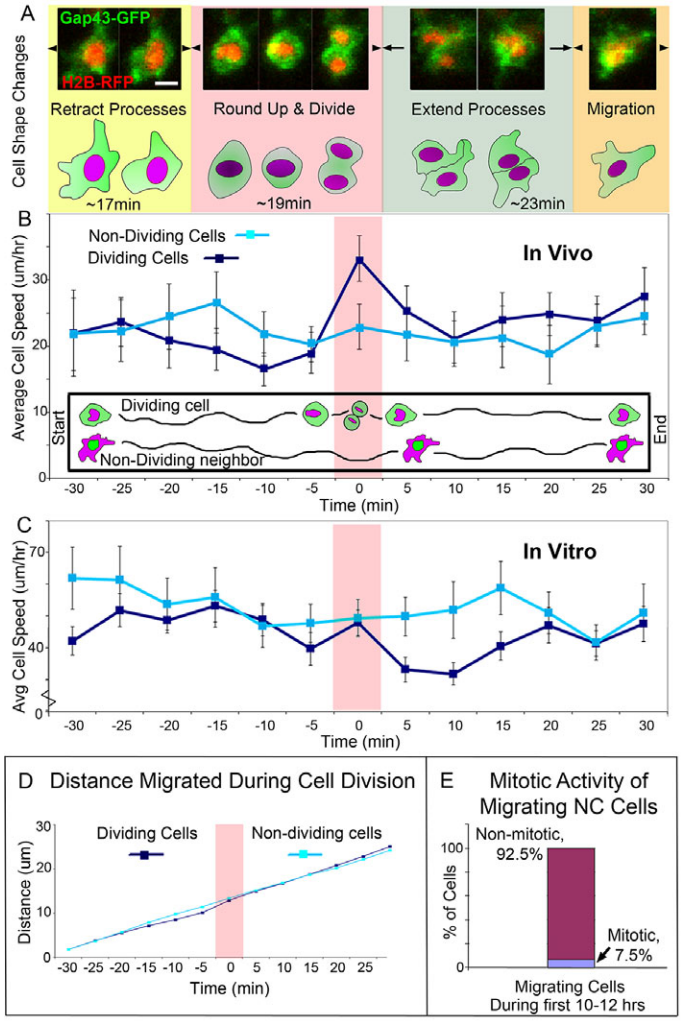

Fig. 1. Neural crest cell division dynamics. (A) Series of stereotypical events that characterize a cranial NC cell division event. (B,C) The average cell speed profiles of dividing (n=38 cells *in vivo*, 44 cells *in vitro*) and non-dividing (n=38 cells *in vivo*, 22 cells *in vitro*) NC cells for (B) *in vivo* and (C) *in vitro* conditions. (D) The distance migrated by dividing and non-dividing NC cells. (E) The percentage of mitotically active migrating NC cells during the initial 10-12 hours of migration (n=534 cells). NC cells are labeled with Gap43-GFP (green) and H2B-mcherry (red). Scale bar: 10 µm.

Dividing neural crest cells maintain their spatial order with respect to non-dividing neighbors

To determine whether dividing NC cells disrupt spatial order in the stream, we measured cell speed profiles prior to, during and after a cell division event (Fig. 1B, dark blue line, n=38). We also examined the speed of neighboring, non-dividing NC cells that traveled within 30-50 µm (two to three cell diameters) of a dividing NC cell (Fig. 1B, light blue line, n=38). We found a slight, non-significant, decrease in the speed of dividing NC cells just prior to cell division (Fig. 1B). This resulted in a minimal loss in distance traveled compared with non-dividing neighbors (Fig. 1D). This subtle spatial disadvantage was compensated for by an increase in cell speed at the time of cytokinesis (Fig. 1A,B), due to a rapid physical separation of the daughter nuclei. Thus, dividing NC cells, which were only ~7.5% of the total number of migrating NC cells at the early phase of migration (Fig. 1E, n=534 total cells), maintained their spatial position in the migratory stream, despite undergoing a mitotic event (Fig. 1D). Similarly, we did not observe significant differences in the NC cell speed profile of dividing versus non-dividing NC cells in *in vitro* cultures prior to division (Fig. 1C). However, the data (Fig. 1C) show that dividing NC cells in culture moved significantly slower in the first 15 minutes after cytokinesis. Together, this suggests NC cell speed prior to and during division is independent of tissue growth, but the ability of dividing NC cells to maintain speed in the embryo following division may be influenced by tissue dynamics.

Neural crest cell division orientation was random with no preference to dividing in the direction of migration

To determine whether there is a bias in the orientation of cranial NC cell divisions, we analyzed NC cell division plane angles in migrating cells (Fig. 2A,B; plane constructed between two dividing cell progeny measured from 0-90°). For example, division plane orientation perpendicular (perp) to the direction of migration would suggest that mitosis may contribute to expansion of the migratory stream in the direction of the target. When we measured the division

Development (2014) doi:10.1242/dev.098855

Table 1. Average time (in minutes) dividing, migratory neural crest cells spend in the various stages of the mitotic sequence

Phenotype	Average time±s.e.m. (minutes)
Retract filopodia and round up	17.2±2.2
Divide after rounding up	19.0±1.8
Extend filopodia to pre-division lengths	23.0±3.7
Total length of mitosis	59.2±6.0

The average mitosis took approximately 1 hour (*n*=19).

plane angles in relation to the direction of the NC cell migratory pathway (Fig. 2A), we found that nearly 58% of mitotic NC cells (23/40) had a division plane angle perpendicular to the stream direction. The remaining 42% (17/40) of cells had a division plane angle parallel (para) to the stream direction (Fig. 2B; supplementary material Movie 2). This slight tendency was not significantly different from a random distribution (chi-squared=0.34). We also found that both lead and trailing cranial NC cell subpopulations within a typical migratory stream displayed similar cell division orientation measurements (Fig. 2B). Together, this suggests that cranial NC cell division orientation angles during migration are random and not regionally distinct within a stream.

Neural crest cell distance migrated and time to first division after neural tube exit were stochastic

To determine whether there is a spatiotemporal pattern to the first division of cranial NC cells, we tracked cells after neural tube exit and marked the time and location of cell divisions (Fig. 2C). If NC cells were synchronized prior to delamination from the neural tube or after encountering microenvironmental signals, we would expect to see a pattern to the location and/or time of the first division. We learned that cranial NC cells divided over a wide range of times, including as early as 35 minutes and as late as 13.3 hours, after exiting the neural tube (Fig. 2C, top, *n*=36 cells). We observed no significant difference in the time to first division between lead and trailing NC cell subpopulations (Fig. 2C, top, compare purple and green diamonds). We also measured the displacement of NC cells after neural tube exit and found that cells could divide within one cell diameter (~15 µm, immediately after exit) or as far as 180 µm from the neural tube exit point (Fig. 2C, bottom, *n*=35 cells). Thus, both the time and distance a NC cell traveled prior to its first division appeared to be unpredictable.

Neural crest cell mitotic activity significantly increased as cells entered the branchial arches

To examine NC cell division events as cells entered head target regions, we performed BrdU analysis of GFP-transfected NC cells at different developmental stages (E2-E3.5) during cranial NC cell migration (Fig. 3A-C). We found a significant difference in BrdU incorporation within lead NC cells at the migratory front compared with the trailing subpopulation at E3.5 (Fig. 3D, blue line compared with red line; *P*=0.05). In the front 30% of streams (700-1000 µm), 32.4±3% of GFP-positive cells were also BrdU positive (Fig. 3D, blue line, *n*=5 embryos, 816 cells). However, in the trailing 70% of streams (0-700 µm), only 20.6±3% of NC cells were BrdU positive (Fig. 3D, red line, *n*=5 embryos, 1434 cells). There were no significant differences in the number of BrdU-labeled NC cells at earlier stages (E2-E3; data not shown). This suggests that lead NC cells increase mitotic activity after entering the branchial arches.

To better define the time and location associated with mitotic activity of cranial NC cells during the homing to and target invasion

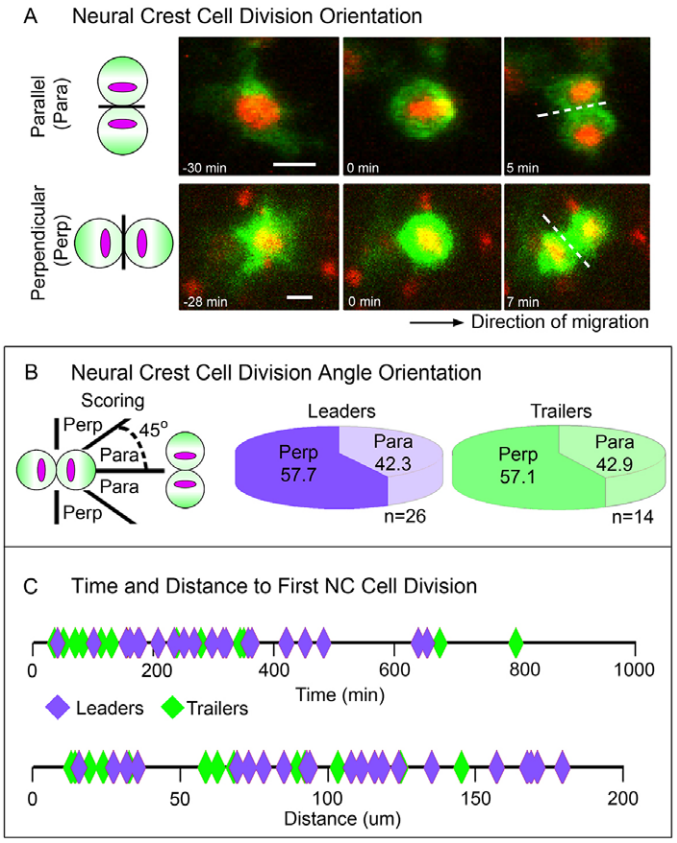

Fig. 2. Neural crest cell division orientation and time and distance to first division. (A) Examples of typical dividing NC cells with an angle of division either parallel or perpendicular to the direction of migration. (B) NC cell dual color labeling (Gap43-GFP, green; H2B-mcherry, red) provided scoring of cell division orientation, with respect to the direction of migration. Graphs showing the percentage of parallel or perpendicular orientation angles in dividing lead and trailing NC cells. (C) Measurements of the time (top, *n*=36 divisions) and distance (bottom, *n*=35 divisions) to first NC cell division. Scale bars: 10 µm.

phases of migration, we photoconverted single and small numbers of migrating mKikGR-labeled NC cells (Fig. 4A-F). mKikGR is a monomeric version of KikGR, a photoswitchable fluorescent protein capable of changing the chromophore emission wavelength from a green-to-red signal, upon UV excitation (Habuchi et al., 2008). Between 12 and 24 hours after electroporation of HH9 stage embryos, we found that, on average, a single lead cranial NC cell would become 1.7±0.3 cells (Fig. 4A-C,G, *n*=7 embryos, 20 cells). Strikingly, between 24 and 36 hours after electroporation, a single lead NC cell gave rise, on average, to 6.0±1.0 cells (Fig. 4D-F,G, *n*=7 embryos, 30 cells). Analysis of single lead NC cells on a cell-by-cell basis showed no evidence of isolated, super proliferating individuals (Fig. 4H). Photoconversion of cells within the trailing population 24 hours after electroporation of mKikGR at the same developmental stage, followed by reincubation for an additional 12 hours showed that, on average, a single NC cell gave rise to 2.3±0.5 cells (Fig. 4G, *n*=9 embryos, 55 cells).

Analysis of photoconverted NC cell divisions allowed us to calculate differences in average NC cell doubling times depending on the cranial NC cell phase of migration (Fig. 4G; Table 2). We found that early emerging lead NC cells had an average doubling time of 16.2 hours (Fig. 4G; 12-24 hours). After populating the branchial arches, lead NC cells showed a significantly shorter

Development (2014) doi:10.1242/dev.098855

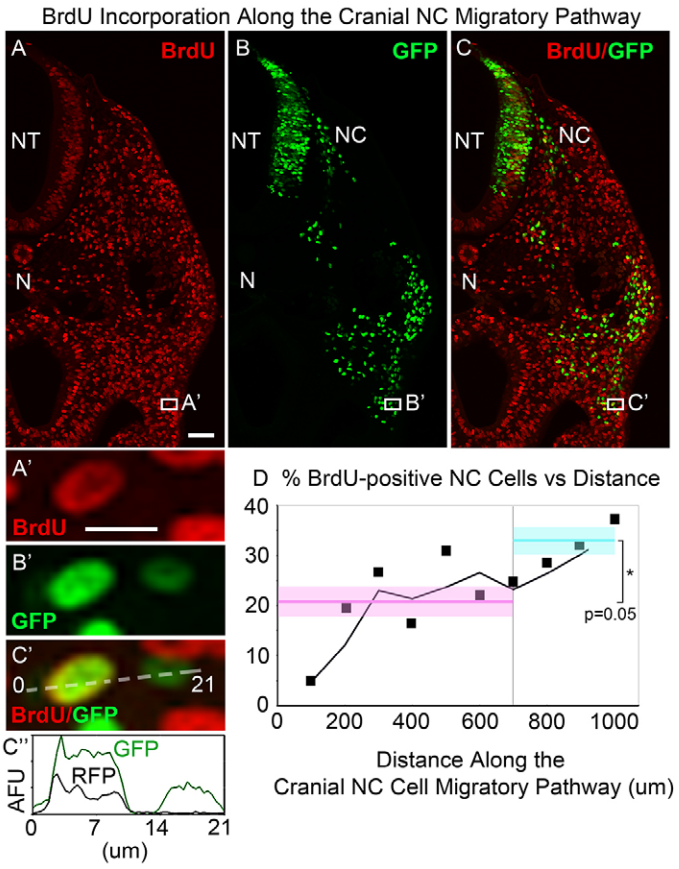

Fig. 3. BrdU labeling reveals proliferating NC cells along the migratory pathway. (A-C) A typical transverse section through the hindbrain rhombomere 4 (r4) level of an E3.5 chick embryo during NC cell migration showing the dorsal region of the tissue section on one side of the embryo. (A,A′) BrdU-positive cells (red), (B,B′) GFP-labeled NC cells (green) and (C,C′) colocalized BrdU-positive NC cells (overlay) are shown. (A′-C′) Magnified views of a small subset of cells from A-C showing an example of a BrdU-positive NC cell (red and green signal) and BrdU-negative NC cell (green with no red signal). (C″) Line intensity profile through two neighboring cells in C over 0-21 μm (measured left to right) showing the bi-modal peaks of GFP (indicating both cells are GFP-positive NC cells) and single peak RFP (indicating only one of the cells has a red fluorescence signal and is BrdU positive). (D) The average percentage of BrdU-/GFP-positive NC cells measured along the migratory pathway (0-1000 μm) and binned into 100 μm intervals (squares; *n*=5 embryos, 2204 total cells). The black line represents the moving average of two neighboring measurements (interval of 400 μm) of BrdU-/GFP-positive NC cells (squares). The red line and shaded area represent the average percentage of BrdU-positive cells (±s.e.m.) in the trailing subpopulation (0-700 μm, 20.6±3%). The blue line and shaded area represent the average % BrdU-positive cells (±s.e.m.) in the lead population (700-1000 μm, 32.4±3%). Scale bars: 50 μm in A; 10 μm in A′.

doubling time of only 4.6 hours (Fig. 4G; 24-36 hours). By contrast, trailing NC cells over this same time period (24-36 hours) had a doubling time of 9.9 hours. Thus, even within the same NC cell migratory stream, cells displayed a more than twofold difference in doubling time depending on position within the lead or trailing subpopulations.

Reduction in premigratory neural crest cells led to increased proliferation of remaining migrating cells

To address whether the number of migrating NC cells would affect individual cell proliferation, we ablated the dorsal one-third of the neural tube (containing premigratory NC cells from approximately mid-r3 to mid-r5) after less than 10 fluorescently labeled NC cells were observed to have emigrated (Fig. 4I). By performing this ablation, we significantly reduced the number of migrating NC cells and observed changes to remaining NC cell behaviors. Confocal time-lapse analysis of the migrating NC cells revealed a significant increase in the rate of dividing cells compared with control pseudo-ablated embryos in which the excised tissue was re-placed (Fig. 4I, P=0.0052). In ablated embryos (n=3), migrating NC cells divided at a rate of 5.6±0.5% per hour (Fig. 4I, n=83 cells). By contrast, in time-lapse movies of control pseudo-ablated embryos (n=4), 2.6±0.4% of migrating NC cells divided per hour (n=97 cells). These results suggest that NC cell density within a migratory stream influences cell proliferative activity.

FACS analysis revealed significant differences in neural crest cell cycle profiles during migration

To address the relationship between cell cycle profile and NC cell position within a stream further, we performed FACS analysis (Fig. 5A-H) and Ki-67 staining (Fig. 5I-K) of HNK-1-positive NC cells at 8, 16, 24 and 32 hours after microinjection and electroporation of EGFP into HH9 stage embryos. We found significant differences in cell cycle profiles between lead and trailing NC cell subpopulations (Fig. 5G,H). First, the cell cycle profile of lead NC cells remained consistent over time. Slightly more than 30% of NC cells were in G1 phase shortly after exiting from the neural tube (Table 3, 31.2±1.3% at the 8-hour time point, n=4). This percentage remained stable within the lead NC cell subpopulation at all time points examined [35.3±2.3% (16 hours, n=8), 33.4±5.7% (24 hours, n=4) and 34.6±2.1% (32 hours, n=8), respectively (Table 3; Fig. 5G,H)]. By contrast, the cell cycle profile of the trailing NC cell subpopulation was similar to the lead NC cell cycle profile at early time points [Table 3; Fig. 5G; 30.3±1.6% (16 hours, n=8)]. However, this rose to nearly 40% at the 24-hour time point (39.4±2.3%, Table 3; Fig. 5H, n=4). By 32 hours, more than 50% of trailing NC cells were in G1 (50.6±1.8%, Table 3; Fig. 5H, n=8).

We also performed Ki-67 staining to assess the number of actively cycling cells within each subpopulation (Fig. 5I-K). This analysis revealed that more than one out of every five cells (21.2±5.0%) in the trailing NC cell subpopulation at 32 hours had exited the cell cycle (Fig. 5I,J, n=3). By contrast, only 4.7±2.4% of lead NC cells had exited the cell cycle (Fig. 5I,K, n=3). Together, these data show that lead and trailing cranial NC cell subpopulations have distinct cell cycle profiles that diverge as early as 24 hours after neural tube exit.

DISCUSSION

We used the chick cranial neural crest (NC) system to study the details of cell division during migration and determine how cell cycle is related to phases of migration in the embryo. Our results revealed several key features of individual cell division events and the pattern of cell cycle changes during distinct phases of cranial NC migration. Dividing NC cells underwent a rapid, stereotypical sequence of cell shape changes that lasted 1 hour, during which the cells did not dramatically slow down or lose position with respect to non-dividing neighbors. The time and distance migrated from neural tube exit to the first division was unpredictable and NC cells divided without a preferred division orientation angle. NC cell mitotic activity was relatively quiescent during migration, but could be stimulated when the number of migrating cells was decreased by tissue ablation. There were also significant changes in NC cell cycle

Development (2014) doi:10.1242/dev.098855

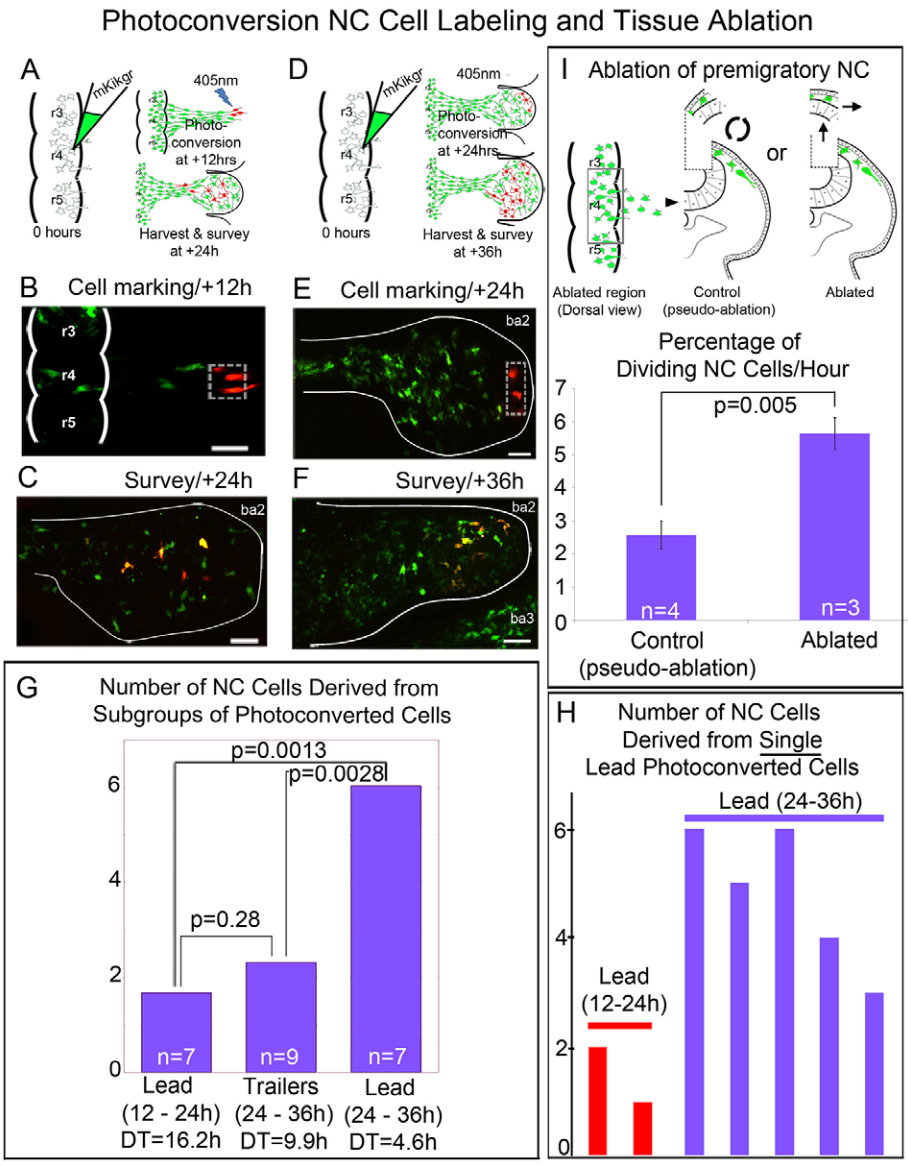

Fig. 4. Photoconversion cell labeling and tissue ablation show differences in NC cell proliferative activity depending on NC stream position, migratory phase and stream density. (A-F) Schematic and example images showing photoconversion of mKikGR-labeled NC cells within a typical cranial NC cell stream. (B,E) Small numbers of NC cells were photoconverted (dashed box) at +12 hours and +24 hours after labeling premigratory NC cells with mKikGR. (C,F) Embryos were re-incubated for an additional +12 hours and the total number of photoconverted cells and progeny were measured. (G) Graph showing the number of cells derived from photoconverted migrating NC cells and doubling times at two distinct time points and from either lead or trailing subpopulations of the NC migratory stream. DT, doubling time. (H) Photoconversion of single lead NC cells (at +12/+24 hours after mKikGR-labeling or premigratory cells) and number of cell progeny derived from single photoconverted NC cells (measured at +12 hours). (I) Schematic of tissue ablation of later emerging premigratory NC cells at the mid-hindbrain level and percentage of dividing NC cells per hour measured from *in vivo* confocal time-lapse imaging data (n=7 time-lapse imaging sessions). The embryos are the same in B,C and E,F. Scale bars: are 50 µm in B,C,E,F.

profile, depending on the migratory phase and stream position. Lead NC cells dramatically increased their mitotic activity and trailing NC cells tended to exit the cell cycle after reaching their distal and proximal target regions, respectively.

Cranial neural crest cell proliferation dynamics

In the absence of time-lapse data, it was unclear what effects proliferating cranial NC cells would have on migratory stream dynamics. Previous analyses of other embryonic migratory patterns have shown that endothelial cells significantly slow down during mitosis and are leap-frogged by non-dividing neighbors (Sato et al., 2010). Static data from chick enteric NC cell migration also described cell leap-frogging during cell division events within the migratory front (Simpson et al., 2007). Thus, we expected to visualize similar cranial NC cell behaviors. However, we observed that cranial NC cells displayed a rapid cell division sequence of reproducible cell shape changes, but dividing cells did not lose position with respect to non-dividing neighbors (Fig. 1B,D). There are at least two possible explanations for this. The rapid 1 hour period over which cranial NC cells divided was comparable with their average cell speed. That is, over 1 hour, non-dividing NC neighbors do not separate too far from each other (Fig. 1A,B). Second, there were few cranial NC cell divisions during the early migration phase, within 12 hours after neural tube exit (Fig. 1E; n=7.5% of migrating cells). Thus, the rapid neural crest cell division sequence with respect to average cell speed, fewer cell

Table 2. Doubling times of various populations of NC cells based on photoconversion experiments

Cell population	Time after NT exit (hours)	Number of divisions in 12 hours	Doubling time (hours)
Early emerging NC cells (n=7 embryos, 20 cells)	12-24	0.74	16.2
Trailing NC subpopulation (n=9 embryos, 55 cells)	24-36	1.21	9.92
Lead NC subpopulation (n=7 embryos, 30 cells)	24-36	2.59	4.63

The number of divisions per 12 hours was determined using the general equation for cell proliferation [N(t) = N(0)*2^(kt)].

Development (2014) doi:10.1242/dev.098855

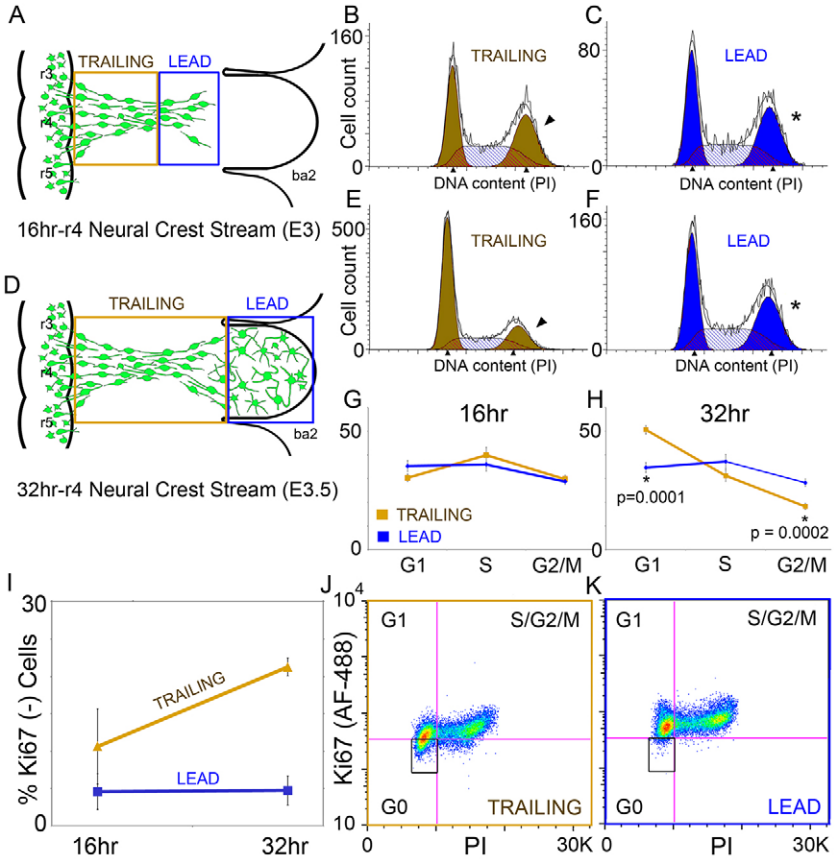

Fig. 5. FACS and Ki-67 analysis reveal distinct cell cycle profiles of lead and trailing neural crest cells. (A,D) Schematic of the lead and trailing subregions of a typical cranial NC cell migratory stream selected for FACS and Ki-67 analysis. (B,C,E,F) Distribution of cells in G1 and G2/M phases of the cell cycle; cells in S phase are located between the two peaks and are represented by the hatched curve, as determined using Modfit software. (G,H) The cell cycle phase distribution of NC cells from both the lead and trailing subpopulations of a typical cranial NC cell migratory stream (n=8 at each time point). (I-K) The percentage of Ki-67 negative cells in the lead and trailing NC cell subpopulations (n=4 at 16 hours and n=3 at 32 hours), showing a significantly higher percentage of Ki67$^-$ cells in the trailing population (P=0.041).

divisions during migration, and maintenance of cell position with respect to non-dividing neighbors suggests that cell division during migration does not affect overall cranial NC cell stream dynamics.

Whether cranial NC cell division orientation promotes directed stream migration was unclear. Preferential NC cell division orientation would act to position daughter cells along the direction of migration so that each division lengthened the rank of cells (Fig. 2B; perpendicular). Studies in zebrafish gastrulation have shown that cells in dorsal tissues preferentially divide along the animal-vegetal axis of the embryo (Gong et al., 2004) and may be coupled with cell rearrangements and cell shape changes to drive axis elongation (Quesada-Hernández et al., 2010). Within the chick primitive streak, oriented cell divisions play a role in streak elongation (Wei and Mikawa, 2000). Thus, we anticipated the possibility there might be oriented cranial NC cell divisions. However, our finding that cranial NC cell division orientation was random (Fig. 2B) supports the idea that cell division events are independent from overall directed stream migration.

The role of the cell cycle in phases of cranial neural crest cell migration

Our results revealed that cranial NC cell divisions occurred in a stochastic manner after neural tube exit, suggesting that cells are not synchronized to divide by signals within the neural tube or by a specific microenvironmental cue along the migratory pathway (Fig. 6B). That is, if cranial NC cells are synchronized in the cell cycle during neural tube exit, we would expect the first division to occur within a time window (Fig. 6B, green box) between measured average NC cell speeds (Fig. 6B, top and bottom lines). Alternatively, if cranial NC cell divisions are triggered by a microenvironmental cue encountered along the migratory pathway, we would expect the pattern of cell divisions to lie within a spatial window (Fig. 6B, orange box). Instead, we observed no pattern to the time and distance to first cranial NC cell division (Fig. 2C; Fig. 6B, blue diamonds). Our data fit well with a previous analysis of cranial NC cell delamination that showed chick cranial NC cells exit the dorsal neural tube independent of cell cycle phase (Théveneau et al., 2007). Thus, we interpret our data to suggest that

Table 3. Percentage of cells of each population that is in the respective cell cycle phase

Condition	G1 (±s.e.m.)	S (±s.e.m.)	G2/M (±s.e.m.)
8 hour NC cells	31.2±1.3	47.3±4.2	21.5±3.6
16 hour lead	35.3±2.3	35.9±2.8	28.8±1.2
16 hour trailing	30.3±1.6	39.9±3.3	29.8±1.7
24 hour lead	33.4±5.7	42.8±6.1	23.8±3.8
24 hour trailing	39.4±2.3	38.8±2.8	21.8±0.9
32 hour lead	34.6±2.1	37.2±3.0	28.2±1.6
32 hour trailing	50.6±1.8	31.2±2.4	18.2±1.3

Data were taken from n=4 experiments (8 and 24 hours) or from n=8 experiments (16 and 32 hours).

Development (2014) doi:10.1242/dev.098855

cranial NC cells exit the neural tube in random phases of the cell cycle and divide in a stochastic manner unrelated to a specific microenvironmental signal(s).

Whether the lack of cell division patterns and the relationship between cell cycle and migratory phase is re-capitulated in the post-otic and trunk regions is less clear. Static studies have shown that chick trunk NC cells undergo a G1/S transition in the dorsal neural tube prior to neural tube exit (Burstyn-Cohen and Kalcheim, 2002). However, recent *in vivo* time-lapse imaging studies in chick in our lab revealed that trunk NC cells may remain resident in the neural tube after moving to the dorsal midline, and that these NC cells are capable of dividing within minutes after neural tube exit (McKinney et al., 2013). Thus, trunk NC cells may undergo a G1/S transition, but not immediately exit the neural tube. Together, this suggests that NC cells do not have synchronized cell cycles before exit from all along the vertebrate axis and divide in a random pattern during early migration phases.

Cranial NC cell mitotic activity was surprisingly quiescent during the early phases of migration (0-12 hours after neural tube exit; Fig. 1E), with only 7.5% of NC cells undergoing mitosis. This raised the possibility that signals within the neural tube or along the migratory route suppress the ability of a cranial NC cell to respond to mitogenic factors. For example, signals endowed by the neural tube on premigratory cranial NC cells may sequester cell cycle progression during migration, but leave cells poised to rapidly respond to mitogenic factors rapidly after entering target branchial arches. This signal(s) is currently unknown. Our photoactivation data (which represented a much cleaner means to measure individual cell proliferation) clearly showed that cranial NC cells did respond to rapidly decrease cell cycle time from 16 hours to 4.5 hours during branchial arch target invasion (Fig. 4G; Fig. 6A,B). Alternatively, NC cell stream density may also affect cell proliferation. Our tissue ablation experiments that decreased the number of migratory cranial NC cells showed a dramatic increase in the number of dividing NC cells along the migratory pathway (Fig. 4I). The earliest time point at which a significant increase in mitotic activity could be detected in ablated embryos was 5 hours after ablation, from time-lapse imaging sessions lasting between 5 and 12 hours (Fig. 4I). Thus, signals that suppress cranial NC cell mitotic activity may be cell density related or altered following neural fold ablation.

The quiescent mitotic activity of cranial NC cells during early phases of migration is in sharp contrast with enteric NC cell behaviors. During enteric nervous system patterning, NC cells invade the gut by rapidly dividing within the migratory front (Simpson et al., 2007). One explanation for the difference in cranial versus enteric NC cell mitotic activity during migration may be related to gut biology. Enteric NC cells must populate the entire length of the gut rather than only discrete proximal and distal locations. Enteric NC cells may simply respond to mitogenic factors during all phases of migration in order to pattern the entire length of the gut, rather than only after reaching discrete target sites such as in the head. Thus, the NC cell cycle may be regulated differently depending on the region of migration and local patterning signals.

Our observed quiescence of cranial NC cell proliferation during early phases of migration may be comparable with other embryonic and cancer cell invasion patterns. Studies in cancer metastasis have suggested there is a delicate balance between cell proliferation and invasion, referred to as ‘Go or Grow’ (Giese et al., 1996; Hoek et al., 2008). The ‘Go or Grow’ hypothesis proposes that cell division and cell migration are temporally exclusive events and that tumor cells defer cell division to migrate (Gil-Henn et al., 2013; Hoek et al., 2008; Rubio, 2007). Similarly, during embryonic development of *C. elegans*, anchor cells appear to be maintained in a post-mitotic state to encourage differentiation into an invasive cell (Matus et al., 2010). Thus, further insights into how NC cells escape the effect of mitogenic signals during particular phases of migration may have implications to other developmental and cancer cell invasion models.

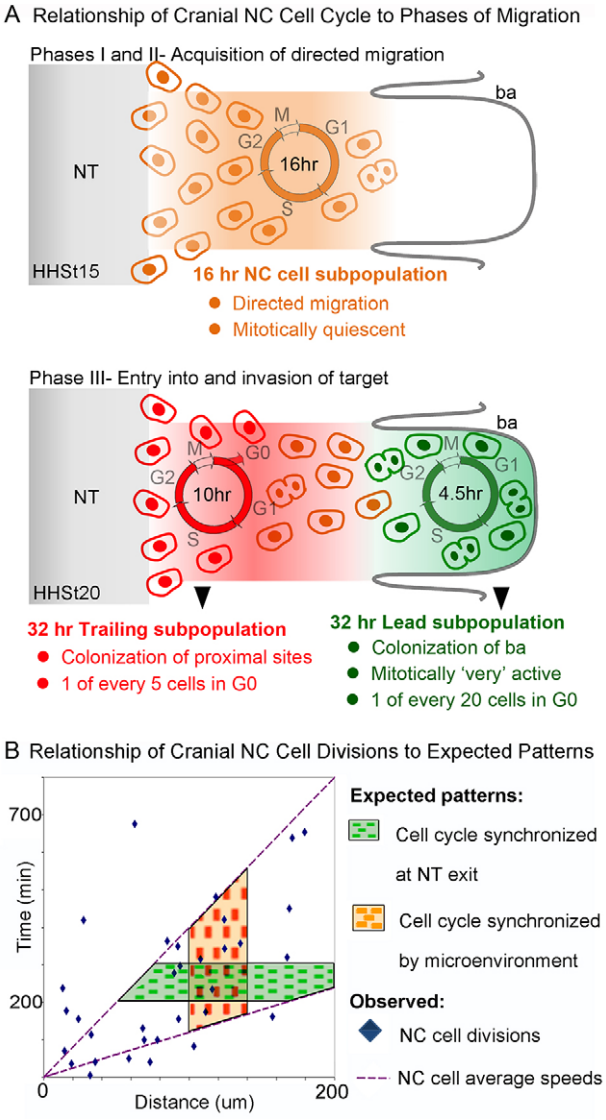

Fig. 6. Models of the relationship of cranial NC cell cycle to phases of migration and expected patterns of cell division. (A) Phases I and II show a 16-hour NC cell cycle and relative mitotic quiescence. In Phase III of cranial NC cell migration; lead NC cells are mitotically very active (4.5-hour cell cycle). Trailing NC cells have an average 10-hour cell cycle, but a significant number of these cells (21.2%) enter G0. (B) Representation of the relationship between cranial NC cell cycle and measurements of the time and distance to first NC cell division. If cranial NC cells are synchronized during neural tube exit, the first cell division should occur within a time window (green box) that fits within a range of average measured cranial NC cell speeds (top line=15 μm/hour; bottom line=40 μm/hour). The orange box designates the subregion where NC cell divisions should occur if a microenvironmental signal(s) triggers NC cell proliferation. The blue diamonds represent the actual observed cranial NC cell divisions measured within the space/time window showing a stochastic nature to the cell division events and no preference to lie within either the green or orange boxes.

Development (2014) doi:10.1242/dev.098855

Summary

This study has revealed important insights into the cellular mechanisms that underlie NC cell cycle progression and cell division dynamics during migration (Fig. 6). We postulate that the cranial NC cell cycle is differentially regulated depending on the phase of migration and cell position within a migratory stream. NC cells migrate in a quiescent, relatively non-proliferative state following neural tube exit (Fig. 6A). NC cells that reach presumptive target tissues either rapidly speed up cell cycle progression or exit the cell cycle depending on target location (Fig. 6A). We propose there is a close relationship between the regulation of individual NC cell division dynamics and the multicellular context of NC cell patterning during migration. Further studies using the NC model will help shed light on the mechanistic nature of how signals regulate a cell's entrance into and exit from a quiescent proliferative state during embryonic development.

MATERIALS AND METHODS

Embryo preparation and in vivo cell labeling

Embryos were prepared as previously described (Kulesa et al., 2008) from fertilized White Leghorn chicken eggs (Phil's Fresh Eggs, Forreston, IL) incubated at 37°C in a humidified incubator until the appropriate stages. Embryos were staged according to well established staging criteria (Hamburger and Hamilton, 1951). Plasmid DNA was transfected into the lumen of the cranial neural tube as previously described (McLennan and Kulesa, 2007).

Time-lapse imaging

Time-lapse confocal imaging was performed as originally described (Kulesa and Fraser, 1998), with minor modifications. Briefly, whole chick embryo explants were visualized using an inverted confocal microscope (LSM 510 NLO and LSM 5 Pascal; Carl Zeiss MicroImaging, Thornwood, NY) with either a 10× NA=0.3 or 0.45 objective (Carl Zeiss). Images were recorded every 5 minutes and image stacks were concatenated and analyzed for playback using both Aim or Zen (Carl Zeiss) software. Movies were created and annotated using NIH ImageJ.

Tissue ablation of premigratory neural crest cells

Tissue ablations were performed *in ovo* ~10 hours after fluorescent cell labeling of premigratory neural crest cells (in HH9 stage embryos) using microinjection and electroporation of Gap43-EYFP. A fine needle was used to excise the dorsal one-third of the neural tube from mid-rhombomere 3 (r3) to mid-r5, at a time shortly after the first migratory neural crest cells (<10 cells) had exited the neural tube, as visualized with a fluorescence dissecting microscope (catalog number MZ10F, Leica Microsystems, Buffalo Grove, IL). Control pseudo-ablation used the same procedure, but the dorsal midline was left intact so as to provide a hinge for the ablated tissue to be gently pulled up and placed back into the cut region.

Cell proliferation dynamics measurements

The time to first division was determined by measuring when a NC cell was first identified (at neural tube exit) until the cell began cytokinesis (indicated by separation of the daughter nuclei). Epithelial-to-mesenchymal transition at the neural tube midline was difficult to observe in these time lapses, so neural tube exit was defined as the time at which a NC cell passed the border of the neural tube (as viewed from the dorsal side of the embryo). The distance to first division was measured as the total displacement of the cell trajectory from neural tube exit until the cell underwent cytokinesis. Division orientation was measured as the angle of the mitotic plane relative to the direction along the NC cell migratory pathway (Fig. 2B). NC cell speed profiles were aligned at the point of division and were calculated using the instantaneous speed of a cell within a 2-hour window of the cell division event. Measurements were scored using AIM (Carl Zeiss) and Imaris (Bitplane AG, Zurich, Switzerland) software.

BrdU analysis

For bromodeoxyuridine (BrdU) incorporation, HH9 stage embryos were electroporated with H2B-EGFP or Gap43-EGFP, and reincubated at 37°C in a humidified incubator until 30 minutes before the desired developmental stage (E2, E3 or E3.5). BrdU Labeling Reagent (30 µl of a 1 µg/ml solution) (catalog number 000103, Invitrogen) was administered directly above the r4 region of each embryo. BrdU immunochemistry was performed using a standard protocol (Rifkin et al., 2000) with a rat monoclonal IgG anti-BrdU (catalog number sc-70441, Santa Cruz Biotechnology, Santa Cruz, CA; 1:500) and Alexa Fluor 633 goat anti-rat IgG (catalog number A21094, Invitrogen; 1:1000).

For analysis, GFP-positive NC cells outside of the neural tube and containing a BrdU-positive nucleus were defined and counted as NC cells that had been in S-phase during the 30-minute BrdU pulse (indicating mitotic activity/cell cycle progression). The number of BrdU-/GFP-positive NC cells were counted and binned in 100 µm intervals along the migratory pathway (~1000 µm in E3.5 embryos) and averaged over the total number of embryos. A moving average calculated the average of the percent BrdU-/GFP-positive cells, measured between two (400 µm) intervals.

Photoactivation cell labeling

Chick embryos (HH9 stage) were microinjected and electroporated with mKikGR (catalog number AM-V0150; MBL International, Woburn, MA) to label premigratory NC cells. Two-photon (Zeiss LSM 710) photoconversion of mKikGR-labeled cells and subsequent imaging/scoring of photoconverted cells and progeny was performed as described previously (Kulesa et al., 2008). For calculation of cell doubling times, we used the general equation for cell proliferation as N(t)=N(0)*2^(kt), where N(0) was equal to the number of initial photoconverted NC cells and 1/k was equal to the cell cycle rate.

FACS analysis of the neural crest cell cycle

Chick embryos (HH9 stage) were screened and re-incubated at 37°C for 8, 16, 24 or 32 hours. The r4 NC cell migratory stream was dissected from each embryo, and in the case of 16-, 24- and 32-hour samples, tissue from the lead (30%) and trailing (70%) portions of the stream was segregated. Each pooled sample was dissociated by multiple passages through a 25-gauge needle and incubation in 0.25% trypsin/EDTA (catalog number T4049, Sigma-Aldrich Corporation, St Louis, MO) for 3 minutes at 37°C. The dissociation reaction was stopped by addition of fetal bovine serum (FBS) and the cells were washed once in PBS with 2% FBS.

To assess cell cycle parameters, cells were stained for 45 minutes on ice with an anti-HNK-1 antibody (catalog number TIB-200, ATCC, Manassas, VA) diluted 1:25-1:200, washed with PBS, and incubated for 20 minutes on ice with APC-anti mouse-IgM secondary antibody (catalog number 406509, BioLegend, San Diego, CA) diluted 1:200. Cells were permeabilized by treatment with Cytofix/Cytoperm (catalog number 554722, BD Biosciences, San Jose, CA) for 5 minutes at room temperature followed by treatment with Cytofix/Cytoperm Plus (catalog number 554715, BD Biosciences) for 10 minutes on ice. After washing, cells were re-suspended in Propidium Iodide (PI) Staining Solution [6.2 ml PBS + 1.92 mg RNase (catalog number R4642, Sigma-Aldrich) + 0.128 mg PI (catalog number P4170, Sigma-Aldrich)] and stained for 1 hour at room temperature, or alternatively, cells were incubated with DAPI (catalog number D3571, Life Technologies, Carlsbad, CA; 1 µg in 250 µl PBS) for 30-60 minutes.

In order to quantify the number of actively cycling cells, we performed Ki-67 analysis. Following treatment with Cytofix/Cytoperm Plus, cells were stained for 30 minutes at room temperature with anti-Ki-67 Alexa Fluor 488 (catalog number 561165, BD Pharmingen) diluted 1:15.

We used a CyAn ADP Analyzer (Beckman Coulter, Brea, CA) or an Influx high speed cell sorter (BD Biosciences; at 12 psi w/100 µm tip) and the percent population of cells in each phase of the cell cycle was determined using FlowJo (Tree star, Ashland, OR) and Modfit (Verity Software House, Topsham, ME) software. Pooled samples contained between 17 and 60 embryos for each experiment, and varying amounts of HNK-1-positive cells, including an average of ~13,000 (8 hour samples),

~9000 (16 hour), ~10,500 (24 hour) and ~21,000 (32 hour) cells per experiment.

Statistical analysis

Chi square values were calculated for Fig. 2B. *P* values for all relevant measurements were calculated using unpaired *t*-tests. Error bars indicate standard error of the mean (s.e.m.).

Acknowledgements

The authors thank Craig Manthe and members of the Kulesa lab for their helpful discussions.

Competing interests

The authors declare no competing financial interests.

Author contributions

P.M.K. conceived the project; P.M.K., D.A.R. and R.M. designed the experiments. D.A.R. and R.M. designed, performed and analyzed the BrdU (D.A.R.), FACS, Ki-67, and tissue ablation static and time-lapse experiments. P.M.K. and R.M. performed the tissue ablations. J.M.T. performed and analyzed the single and multi-cell photoconversion experiments. C.L.S. and J.S.H. performed the cytometry for the FACS and Ki-67 experiments. All authors were involved in data interpretation. P.M.K. and D.A.R. prepared and wrote the manuscript.

Funding

P.M.K. acknowledges funding from the National Institutes of Health (NIH) [1R01HD057922] and the generosity of the Stowers Institute for Medical Research. Deposited in PMC for release after 12 months.

Supplementary material

Supplementary material available online at
http://dev.biologists.org/lookup/suppl/doi:10.1242/dev.098855/-/DC1

References

Abe, T., Sakaue-Sawano, A., Kiyonari, H., Shioi, G., Inoue, K., Horiuchi, T., Nakao, K., Miyawaki, A., Aizawa, S. and Fujimori, T. (2013). Visualization of cell cycle in mouse embryos with Fucci2 reporter directed by Rosa26 promoter. *Development* **140**, 237-246.

Aman, A. and Piotrowski, T. (2011). Cell-cell signaling interactions coordinate multiple cell behaviors that drive morphogenesis of the lateral line. *Cell Adh. Migr.* **5**, 499-508.

Burstyn-Cohen, T. and Kalcheim, C. (2002). Association between the cell cycle and neural crest delamination through specific regulation of G1/S transition. *Dev. Cell* **3**, 383-395.

Carstens, M. H. (2004). Neural tube programming and craniofacial cleft formation. I. The neuromeric organization of the head and neck. *Eur. J. Paediatr. Neurol.* **8**, 181-210, discussion 179-180.

Cordero, D. R., Brugmann, S., Chu, Y., Bajpai, R., Jame, M. and Helms, J. A. (2011). Cranial neural crest cells on the move: their roles in craniofacial development. *Am. J. Med. Genet. A.* **155**, 270-279.

Creuzet, S., Vincent, C. and Couly, G. (2005). Neural crest derivatives in ocular and periocular structures. *Int. J. Dev. Biol.* **49**, 161-171.

d'Amico-Martel, A. and Noden, D. M. (1980). An autoradiographic analysis of the development of the chick trigeminal ganglion. *J. Embryol. Exp. Morphol.* **55**, 167-182.

Gage, P. J., Rhoades, W., Prucka, S. K. and Hjalt, T. (2005). Fate maps of neural crest and mesoderm in the mammalian eye. *Invest. Ophthalmol. Vis. Sci.* **46**, 4200-4208.

Giese, A., Loo, M. A., Tran, N., Haskett, D., Coons, S. W. and Berens, M. E. (1996). Dichotomy of astrocytoma migration and proliferation. *Int. J. Cancer* **67**, 275-282.

Gil-Henn, H., Patsialou, A., Wang, Y., Warren, M. S., Condeelis, J. S. and Koleske, A. J. (2013). Arg/Abl2 promotes invasion and attenuates proliferation of breast cancer in vivo. *Oncogene* **32**, 2622-2630.

Gong, Y., Mo, C. and Fraser, S. E. (2004). Planar cell polarity signalling controls cell division orientation during zebrafish gastrulation. *Nature* **430**, 689-693.

Habuchi, S., Tsutsui, H., Kochaniak, A. B., Miyawaki, A. and van Oijen, A. M. (2008). mKikGR, a monomeric photoswitchable fluorescent protein. *PLoS ONE* **3**, e3944.

Hahn, A. T., Jones, J. T. and Meyer, T. (2009). Quantitative analysis of cell cycle phase durations and PC12 differentiation using fluorescent biosensors. *Cell Cycle* **8**, 1044-1052.

Hamburger, V. (1961). Experimental analysis of the dual origin of the trigeminal ganglion in the chick embryo. *J. Exp. Zool.* **148**, 91-123.

Hamburger, V. and Hamilton, H. L. (1951). A series of normal stages in the development of the chick embryo. *J. Morphol.* **88**, 49-92.

Hoek, K. S., Eichhoff, O. M., Schlegel, N. C., Döbbeling, U., Kobert, N., Schaerer, L., Hemmi, S. and Dummer, R. (2008). In vivo switching of human melanoma cells between proliferative and invasive states. *Cancer Res.* **68**, 650-656.

Kouskoura, T., Fragou, N., Alexiou, M., John, N., Sommer, L., Graf, D., Katsaros, C. and Mitsiadis, T. A. (2011). The genetic basis of craniofacial and dental abnormalities. *Schweiz. Monatsschr. Zahnmed.* **121**, 636-646.

Kulesa, P. M. and Fraser, S. E. (1998). Segmentation of the vertebrate hindbrain: a time-lapse analysis. *Int. J. Dev. Biol.* **42**, 385-392.

Kulesa, P. M. and Gammill, L. S. (2010). Neural crest migration: patterns, phases and signals. *Dev. Biol.* **344**, 566-568.

Kulesa, P. M., Teddy, J. M., Stark, D. A., Smith, S. E. and McLennan, R. (2008). Neural crest invasion is a spatially-ordered progression into the head with higher cell proliferation at the migratory front as revealed by the photoactivatable protein, KikGR. *Dev. Biol.* **316**, 275-287.

Kulesa, P. M., Bailey, C. M., Kasemeier-Kulesa, J. C. and McLennan, R. (2010). Cranial neural crest migration: new rules for an old road. *Dev. Biol.* **344**, 543-554.

Landman, K. A., Fernando, A. E., Zhang, D. and Newgreen, D. F. (2011). Building stable chains with motile agents: Insights into the morphology of enteric neural crest cell migration. *J. Theor. Biol.* **276**, 250-268.

Le Douarin, N. M. and Kalcheim, C. (1999). *The Neural Crest*. Cambridge: Cambridge University Press.

Matus, D. Q., Li, X. Y., Durbin, S., Agarwal, D., Chi, Q., Weiss, S. J. and Sherwood, D. R. (2010). In vivo identification of regulators of cell invasion across basement membranes. *Sci. Signal.* **3**, ra35.

McKinney, M. C., Fukatsu, K., Morrison, J., McLennan, R., Bronner, M. E. and Kulesa, P. M. (2013). Evidence for dynamic rearrangements but lack of fate or position restrictions in premigratory avian trunk neural crest. *Development* **140**, 820-830.

McLennan, R. and Kulesa, P. M. (2007). In vivo analysis reveals a critical role for neuropilin-1 in cranial neural crest cell migration in chick. *Dev. Biol.* **301**, 227-239.

Quesada-Hernández, E., Caneparo, L., Schneider, S., Winkler, S., Liebling, M., Fraser, S. E. and Heisenberg, C. P. (2010). Stereotypical cell division orientation controls neural rod midline formation in zebrafish. *Curr. Biol.* **20**, 1966-1972.

Ridenour, D. A., McKinney, M. C., Bailey, C. M. and Kulesa, P. M. (2012). CycleTrak: a novel system for the semi-automated analysis of cell cycle dynamics. *Dev. Biol.* **365**, 189-195.

Rifkin, J. T., Todd, V. J., Anderson, L. W. and Lefcort, F. (2000). Dynamic expression of neurotrophin receptors during sensory neuron genesis and differentiation. *Dev. Biol.* **227**, 465-480.

Rubio, C. A. (2007). Further studies on the arrest of cell proliferation in tumor cells at the invading front of colonic adenocarcinoma. *J. Gastroenterol. Hepatol.* **22**, 1877-1881.

Sakaue-Sawano, A., Kurokawa, H., Morimura, T., Hanyu, A., Hama, H., Osawa, H., Kashiwagi, S., Fukami, K., Miyata, T., Miyoshi, H. et al. (2008). Visualizing spatiotemporal dynamics of multicellular cell-cycle progression. *Cell* **132**, 487-498.

Sato, Y., Poynter, G., Huss, D., Filla, M. B., Czirok, A., Rongish, B. J., Little, C. D., Fraser, S. E. and Lansford, R. (2010). Dynamic analysis of vascular morphogenesis using transgenic quail embryos. *PLoS ONE* **5**, e12674.

Schlosser, G. (2006). Induction and specification of cranial placodes. *Dev. Biol.* **294**, 303-351.

Simpson, M. J., Zhang, D. C., Mariani, M., Landman, K. A. and Newgreen, D. F. (2007). Cell proliferation drives neural crest cell invasion of the intestine. *Dev. Biol.* **302**, 553-568.

Solnica-Krezel, L. and Sepich, D. S. (2012). Gastrulation: making and shaping germ layers. *Annu. Rev. Cell Dev. Biol.* **28**, 687-717.

Sugiyama, M., Sakaue-Sawano, A., Iimura, T., Fukami, K., Kitaguchi, T., Kawakami, K., Okamoto, H., Higashijima, S. and Miyawaki, A. (2009). Illuminating cell-cycle progression in the developing zebrafish embryo. *Proc. Natl. Acad. Sci. USA* **106**, 20812-20817.

Tarbashevich, K. and Raz, E. (2010). The nuts and bolts of germ-cell migration. *Curr. Opin. Cell Biol.* **22**, 715-721.

Théveneau, E., Duband, J. L. and Altabef, M. (2007). Ets-1 confers cranial features on neural crest delamination. *PLoS ONE* **2**, e1142.

Trainor, P. A. (2010). Craniofacial birth defects: The role of neural crest cells in the etiology and pathogenesis of Treacher Collins syndrome and the potential for prevention. *Am. J. Med. Genet. A.* **152A**, 2984-2994.

Wei, Y. and Mikawa, T. (2000). Formation of the avian primitive streak from spatially restricted blastoderm: evidence for polarized cell division in the elongating streak. *Development* **127**, 87-96.

Wu, M., Pastor-Pareja, J. C. and Xu, T. (2010). Interaction between Ras(V12) and scribbled clones induces tumour growth and invasion. *Nature* **463**, 545-548.